Parametric assessment of the effect of oxygenated low carbon fuels in a light-duty compression ignition engine

Antonio García*, Javier Monsalve-Serrano, David Villalta and María Guzmán-Mendoza

CMT - Motores Térmicos, Universitat Politècnica de València, Camino de Vera s/n, 46022 Valencia, Spain

Fuel Processing Technology

Volume 229, May 2022, 107199

https://doi.org/10.1016/j.fuproc.2022.107199

Corresponding author (*):

Dr. Antonio García (angarma8@mot.upv.es)

Phone: +34 963876574

Abstract

Low carbon fuels (LCF) are proposed as an alternative to help in the reduction of CO_2 emissions from the energy sector, specially related to transportation. These fuels, due to their synthesis process, can generate carbon offsets that mitigate the combustion emissions, while at the same time they can have other properties that reduce criteria pollutants like soot. The current study evaluates the combustion characteristics, performance, and emissions of three LCFs with 100%, 66% and 33% renewable content in volume. The fuels are assessed as drop-in alternatives for diesel, using a baseline calibration present in commercially available vehicles, and with an optimized calibration that targets NOx emissions reductions. The optimized calibration is reached by performing a design of experiments (DOE) that allows to create linear models to observe the engine response based on injection and air management settings for each of the LCFs at three operating conditions. Then the cases with similar combustion phasing are evaluated to determine the settings that can provide the lowest NOx and soot emissions without worsening fuel consumption and engine efficiency. It is found that when the LCFs are used as drop-in alternatives soot emissions are reduced when compared to diesel while brake-specific fuel consumption (BSFC) is increased by nearly 10 g/kWh. In contrast, the optimized calibration achieves average NOx reductions of 44% when compared to diesel. Under both calibrations well-to-wheel CO_2 reductions of nearly 96% are achieved when the fuel with highest renewable proportion is used.

Keywords

Low carbon fuel; OMEx; e-diesel; FT diesel; engine calibration

1 Introduction

Low carbon fuels (LCF) refer to carbon-neutral or carbon-negative fuels. These fuels can be produced with renewable energy or feedstocks [1], falling into the often-used categories of biofuels [2] [3] or e-fuels (also called synthetic fuels) [4]. Particularly synthetic fuels can represent a long-term energy storage vessel for intermittent energy sources [5], converting surplus electricity from low demand periods into easily stored fuels. The main mechanisms to produce e-fuels include the electrolysis of water to split the molecule into H_2 (hydrogen) and O_2 (oxygen) [6], and carbon capture [7] to obtain non-fossil CO_2 which is used to supply the carbon content for the fuel synthesis. Both these processes in the power-to-fuel pathway are electricity intensive and make the use of renewable energy sources crucial to provide benefits in the reduction of CO_2 emissions. Other advantages of these fuels are the capability to be the direct substitution of their fossil counterparts [8] (as is the case with e-diesel or Fischer-Tropsch (FT) diesel [9]), and the promotion of low pollution combustion systems [10].

For compression ignition (CI) engines, FT diesel and Oxymethylene Dimethylethers (OMEx) are promising alternatives to substitute fossil diesel, while maintaining the high efficiency and low fuel consumption of this type of engine. Fischer-Tropsch is a polymerization reaction that can lead to a diesel-like fuel by liquefying and refining hydrocarbons [11]. It has been shown in [12] that FT diesel can have lower brake specific fuel consumption (BSFC), higher thermal efficiency, and lower criteria pollutants than conventional diesel in an unmodified direct injection engine. Results in [13] indicate that blends containing FT diesel promote significantly lower engine exhaust emissions of unburned hydrocarbons (HC) and CO when compared to a blend containing fossil diesel. OMEx, on the other hand, fits into the oxygenated fuel category. Fuel oxygenation is a property that could help break the tradeoff between NOx and soot in CI engines, as it has been proven to promote extremely low soot emissions levels [14] [15] [16], which in turn could potentially lead to a combustion calibration that can be performed closer to stoichiometric conditions which significantly reduce NOx emissions [17]. Additionally, previous studies with both OMEx and FT diesel show CO_2 footprint reductions of up to 69% and 38.5%, respectively, under a dual-fuel concept combustion [18].

LCFs are proposed, in addition to electric vehicles (EV) and hybrid-electric vehicles [19], as an alternative for the de-fossilization of the emissions coming from the transport sector (one of the main producers of greenhouse gas). The combination of strategies to reduce the carbon footprint is more beneficial than focusing on one strategy alone. This is especially true due to the magnitude of the CO_2 reduction required by 2050 to achieve net-zero emissions and prevent global temperature increases [20]. Additionally, the transport sector is responsible for nearly 25% of all CO_2 emissions produced [21]. To reach these goals, relying on an EV-exclusive strategy, without also improving technologies associated to internal combustion engines, would be detrimental. In fact, some predictions indicate that by 2040 EVs will only account 11-28% of the total vehicle fleet [22], extending the use of liquid fuels as the main energy source for light-duty vehicles to at least 2050. In this regard, another aspect that should be considered with care are the criteria pollutant limits that need to be achieved for the continuous use of ICEs. Currently, Europe has Euro 6 as the regulating normative for these pollutants [23], defining limits of NOx, particle matter (PM), HC and CO [24], but the normative is bound to be updated soon [25] to more stringent limits. To mitigate these emissions, advances have been made on combustion strategies [26] [27] and, relevantly, aftertreatment systems (ATS) to maintain pollutants below regulated limits [28]. The most common aftertreatment systems in CI engines are the diesel oxidation catalyst (DOC) for HC and CO pollutants, the diesel particulate filter (DPF) for PM emissions, and the selective catalytic reducer (SCR) to target NOx emissions. Besides the proven efficiencies of these systems [29] [30], they can increase the complexity and expensiveness of the vehicle [31] [32]. The previous reasons make strategies to reduce emissions without having to modify significantly the vehicle's systems highly attractive, especially when dealing with real driving conditions where transient operation modifies the expected emissions [33].

Provided the advantages of LCFs to serve as replacements for fossil fuels without necessarily needing to realize modifications in the engine systems, and vastly reduce ICE CO_2 emissions, in addition to the need to significantly reduce regulated pollutants to preserve human health and environmental conditions, the current work studies the effect on the performance and emissions of a light-duty CI engine of three LCF blends (LCD100, LCD66 and LCD33), and proposes an optimization towards the reduction of NOx emissions. The fuel blends are composed of varying proportions of FT diesel, OMEx and fossil diesel. Due to the presence of OMEx, which has intrinsic potential for low soot emissions, the NOx reduction optimization can be achieved without severely impacting PM values. The work also addresses the impact in CO_2 emissions the fuels have -both in well-to-tank (WTT), tank-to-wheel (TTW) and well-to-wheel (WTW) terms- due to their different degrees of renewable content.

2 Materials and methodology

2.1 Engine characteristics and test cell description

A 4-cylinder commercially available 1.6 L CI engine provided with high-pressure EGR was used to perform this investigation. More information on the engine can be found on Table 1, including the type of injectors and compression ratio. The ECU was originally provided with a baseline diesel B7 calibration, which through an INCA V5.2 virtual environment was modified in 8 main parameters to achieve the desired calibration for the air management and injection systems. The parameters to be controlled during tests were the fuel mass injected, the injection pressure, the start of injection (SOI), the pilot injections fuel volume and dwell times, the in-cylinder cycle air mass and boosting pressure. The EGR is not a directly controlled parameter, however it is a consequence of the variation of the air mass parameter and the boost pressure. Once the air mass and the boost pressure are set, the EGR valve opens or closes to be able to maintain the target value for these parameters; thus, if the air mass is reduced, the EGR will be increased consequently maintaining the boost pressure.

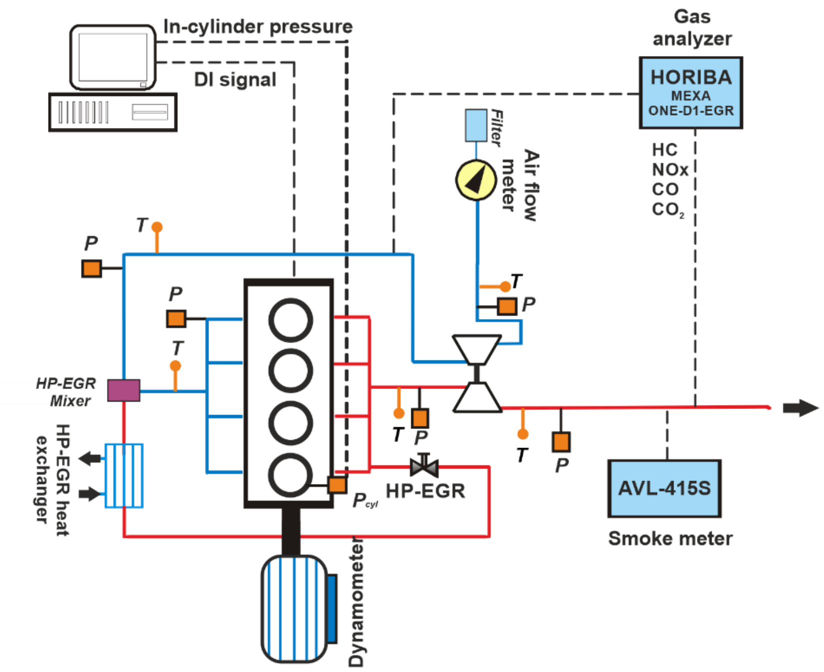

Figure 1. Test cell scheme.

Table 1. Engine characteristics.

General characteristics	
Number of cylinders [-]	4
Cylinder diameter [mm]	79.7
Stroke [mm]	80.1
Total displaced volume [cm^3]	1598
Connecting rod length [mm]	140
Compression ratio [-]	16.0
Rated power [kW]	100 @ 4000 rpm
Rated torque [Nm]	320 @ 2000 rpm

Injection system characteristics	
Type of injector	solenoid
Number of holes [-]	7
Hole diameter [µm]	141
Flow number [FN]	340
Maximum injection pressure [bar]	2000

The engine was installed in a completely instrumented test rig, provided with a Dynas$_3$ LI dynamometer to measure the torque output; a Horiba MEXA 7100 to collect information on the main engine-out emissions of interest (NOx, CO, HC, O_2 and CO_2), as well as calculating the EGR fraction with Equation 1; an AVL 415S smoke meter to measure soot in FSN number; an air flow meter and a fuel balance to measure fuel mass flow. Additionally, pressure and temperature probes were present at the positions identified in Figure 1 and their values were recorded by an in-house LABVIEW controller, called CMT Samaruc, which averaged the measurements. More information on the measuring equipment can be found on Table 2, including the accuracy each instrument has.

$$\%EGR = \frac{CO_{2_{intake}} - CO_{2_{atm}}}{CO_{2_{exhaust}} - CO_{2_{atm}}} \times 100 \qquad \text{Eq. 1}$$

Table 2. Instrumentation accuracy.

Variable measured	Device	Manufacturer/ model	Accuracy
In-cylinder pressure	Piezoelectric transducer	Kistler / 6125C	± 1.25 bar
Intake/Exhaust pressure	Piezoresistive transducers	Kistler / 4045A	± 25 mbar
Temperature	Thermocouple	TC direct / type K	± 2.5 ºC
Crank angle, engine speed	Encoder	AVL / 364	± 0.02 CAD
NOx, CO, HC, O_2 and CO_2	Gas analyzer	Horiba MEXA 7100	4%
FSN	Smoke meter	AVL 415S	±0.025 FSN
Fuel mass flow	Fuel balance	AVL 733S	±0.2%
Air mass flow	Air flow meter	AVL 422	±0.1%
Torque	Dynamometer	$Dynas_3$ LI	±10 rpm ±0.2 %Torque

Uncertainty for measured variables is addressed by measuring each data point three times and calculating the variation from the mean of the measurements (standard deviation). Subsequently, for calculated values, such as break specific values (BSFC, BSNOx, BSSoot, BSHC, BSCO), error propagation analysis was performed following Equation 2, assuming the input variables are statistically independent. In the equation, σ_q is the standard error of a function q, x_i represents the n input variables for the function, and σ_{x_i} is the associated standard error to each input variable.

$$\sigma_q^2 = \sum_i^n \left(\frac{\partial q}{\partial x_i}\sigma_{x_i}\right)^2 \quad \text{Eq. 2}$$

2.2 Fuel characteristics

Three fuels blends with different degrees of renewable content will be evaluated in this study. The fuels are LCD100, LCD66 and LCD33, where the number in their name indicates the proportion of renewable content in volume. Figure 2 shows the fuel blends' compositions where it can be seen that all three fuels contain FT diesel, OMEx and fossil diesel EU. It should be highlighted that the proportion of OMEx in these blends increases with the increase in renewable content and that properties of OMEx are highly influential in the final properties of the blends. Some important properties of the studied fuel blends are present in Table 3. Because the lower heating value (LHV) is different across the fuel blends [34], Equation 3 is used to obtain the equivalent fuel consumption excluding the effect of the LHV and using diesel as the reference and assessing the energy conversion each fuel blend can have; where $\dot{m}$ is the mass flow rate of fuel, and P_{brake} is the brake power.

$$BSFC_{eq}\left[\frac{g}{kWh}\right] = \frac{\dot{m}\cdot\left(\frac{LHV_{fuel\,blend}}{LHV_{Diesel}}\right)}{P_{brake}} \quad \text{Eq. 3}$$

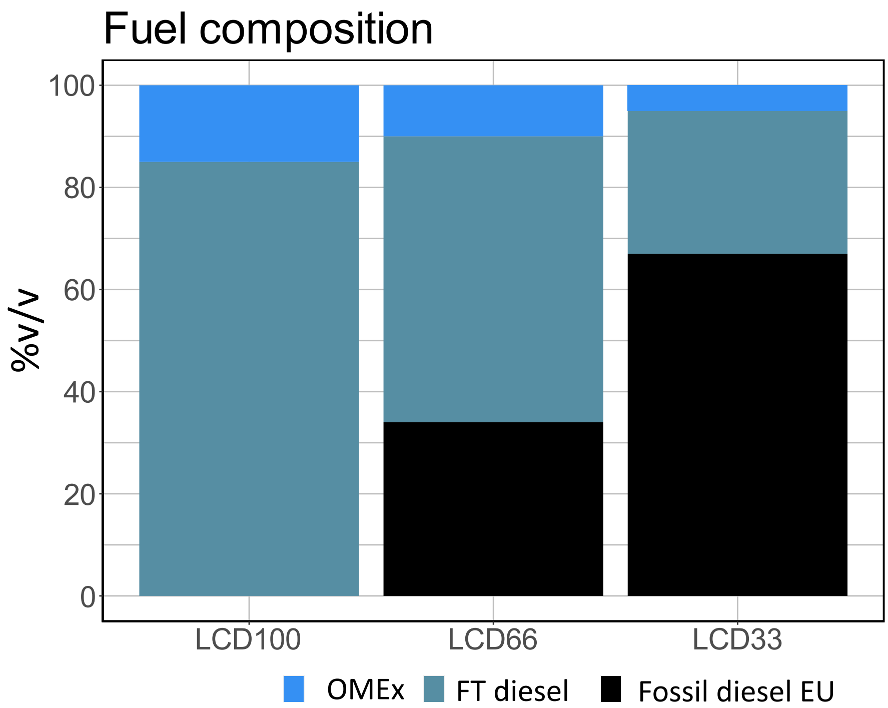

Figure 2. Fuel blend volumetric composition.

It is extensively reported how in CI engines the spray characteristics affect the combustion [35]. Generally, a higher density and viscosity can affect the fuel breakup process (droplet separation) and delay the ignition. However, given the similarity between physical properties of the fuels (as observed in Table 3), with values that are within European specifications, and the use of the same injector for all tests, it is considered that variations in spray characteristics caused by physical properties will be few (similar spray cone angles and penetrations) and combustion delay and phasing variations are more likely caused by the variation of chemical properties. Nonetheless, future dedicated testing is desired to quantify the small variations the proportion of OMEx cause in the spray characteristics and thus in the combustion.

Table 3. Fuel properties at standard conditions.

	Diesel blend	LCD100	LCD66	LCD33	Method
Cetane Index [-]	54.6 ± 0.3	87.0 ± 0.4	70.0 ± 0.4	61.8 ± 0.3	EN ISO 4264
Density @ 15ºC [g/ml]	0.834 ± 0.001	0.821 ± 0.001	0.825 ± 0.001	0.827 ± 0.001	EN ISO 12185
KV @ 40ºC [cSt]	2.86 ± 0.02	2.08 ± 0.01	2.23 ± 0.01	2.46 ± 0.01	ASTM D445
Lower Heating Value [MJ/kg]	42.81 ± 0.02	38.67 ± 0.03	39.96 ± 0.03	41.48 ± 0.02	ASTM D3338 mod
Carbon [% m/m]	85.8 ± 0.1	76.5 ± 0.1	79.5 ± 0.1	82.9 ± 0.1	ASTM D3343 mod
Hydrogen [% m/m]	13.5 ± 0.1	13.8 ± 0.1	13.8 ± 0.1	13.7 ± 0.1	ASTM D3343 mod
Oxygen [% m/m]	0.8 ± 0.1	10.1 ± 0.1	6.8 ± 0.1	3.4 ± 0.1	EN 14078
K_{CO_2} [g_{CO2}/g_{fuel}]	3.22 ± 0.01	2.79 ± 0.01	2.91 ± 0.01	3.04 ± 0.01	Complete combustion assumed
WTT CI [g_{CO2}/MJ]	15.8 ± 0.1	-69 ± 1	-37.1 ± 0.7	-8.2 ± 0.4	[36]

TTW CI [g_{CO2}/MJ]	75.2 ± 0.3	72.2 ± 0.3	72.8 ± 0.1	73.3 ± 0.3	Complete combustion assumed

The fuels' well-to-tank (WTT) carbon intensity was derived from the work performed in [36], while the tank-to-wheel (TTW) CO_2 emissions come from Equations 2 and 3, under the premise of complete combustion. On Equation 4, k_{CO_2} is the coefficient of correlation of a unit of mass of fuel into a unit of mass of CO_2, $y_{C_{fuel\,blend}}$ is the carbon proportion of the fuel in mass, while M_C and M_{O_2} are the molar masses of carbon and oxygen respectively. Then, on Equation 5, $\dot{m}_{CO_2}$ represents the CO_2 mass flow rate. These equations provide a relation between the carbon content in the composition of the fuel and the tailpipe CO_2. The hypothesis is supported, in part, by the high efficiency (above 90% [37] [29]) that can be obtained in diesel oxidation catalysts (DOC) which would make possible the complete oxidation of the fuel after the engine; additionally, this consideration implies the worst-case scenario for CO_2 emissions where all the fuel used in the engine is exhausted from the vehicle as CO_2.

$$k_{CO_2} = y_{C_{fuel\,blend}} \cdot \left(\frac{M_C + M_{O_2}}{M_C}\right) \quad \text{Eq. 4}$$

$$\dot{m}_{CO_2} = k_{CO_2} \cdot \dot{m}_{fuel\,blend} \quad \text{Eq. 5}$$

2.3 Before testing each of the fuel blends, the engine fuel lines and injectors are purged from the reference diesel by maintaining the engine at a medium load operating condition, with constant fuel mass flow and engine speed, and observing the output power. Because the LCFs have a lower LHV, as the diesel is replaced by the LCF the engine output power for the same fuel mass flow is reduced. The fuel line is considered to be completely purged after ten minutes of stationary conditions at the same power output. A similar procedure is done when LCF measurements are finished; the LCFs are purged from the line leaving reference diesel in the engine to guarantee that in future tests with LCFs the testing start is always made with diesel with clearly defined properties and the same LHV relations with the target fuel. Test matrix and statistical modelling

The selected steady-state operating conditions for this study are based on the work of [38]. These operating conditions are distributed across the engine map in such a way that they can be representative of the engine operation during the Harmonized Light Vehicle Test Procedure (WLTP) cycle in a 1600 kg vehicle with a similar engine. Table 4 describes the speed and BMEP for each one of the testing points analyzed in the current work. According to the results from [38], the three selected operating conditions represent 87% of the fuel burned over the WLTP, making the optimization of these particular conditions ideal to provide an overview of the potential of oxygenated fuels under a WLTP scenario.

Table 4. Engine operating conditions.

Test Label	Speed [rpm]	BMEP [bar]	Load [%]
1250 rpm @ 2 bar	1250	2	20
1500 rpm @ 14 bar	1500	14	75
2000 rpm @ 8 bar	2000	8	35

The current work employs linear regression models obtained by evaluating design of experiments (DOE) whose parameters were: injection pressure, start of injection (SOI) timing of the main injection, the volume and dwell of the pilot injections, the charge boost pressure and fresh air mass quantity. The injected fuel mass was fixed during DOE tests to avoid the influence of its variation in the studied responses and other factors like EGR are not considered in the models as they are collinear to the air mass quantity. The responses of interest for each of the different models were the brake specific fuel consumption (BSFC), NOx emissions and soot emissions in brake specific terms, the gross brake efficiency (GBE) and the crank angle degree at which 50% of the heat from combustion has been released (CA50). Similar factors and responses have also been studied in previous DOE work [39], indicating a strong correlation between them and allowing for the optimization of the engine emissions and fuel efficiency.

The test matrix was constructed using two levels and a central point for each of the parameters and, depending on the operating condition, a 2-k factorial design [40] (65 runs), or a modified Plackett-Burman design [41] (32 runs) were employed. Selecting the Plackett-Burman design attended the need to use a shorter test matrix in the 1500 rpm @ 14 bar point, due to the higher load of the condition in order to prevent strain in the testing facility and reduce the possibility of problems like excessive pressure rise rate (PRR) or maximum pressure inside the cylinder beyond 180 bar. The Plackett-Burman design is selected because it allows to observe the response sensitivity to the main factors and have an idea of the possible random measurement errors. In addition, the mentioned modification of the conventional Plackett-Burman included 20 additional custom centrally distributed points to better estimate the variability and improve the prediction capabilities of each of the models, and also reducing confounding effects for the interaction between factors. To select the maximum and minimum testing levels, preliminary studies were performed on each individual parameter to guarantee that NOx emissions remained under 1 g/kWh for the 1250 rpm @ 2 bar condition, 2 g/kWh for the 2000 rpm @ 8 bar one and 3 g/kWh for the 1500 rpm @ 14 bar condition, while soot emission limits were 2 FSN for the lower load condition and 3 FSN for the higher load ones. These preliminary studies ensure that the responses caused by the variation of a single factor are monotonous (either increasing or decreasing), validating the use of a linear modelling approach.

The responses of interest are modelled with polynomial regressions that follow Equation 4, where b_0 is the mean of the analyzed responses, and b_i and b_{ij} represent the effect of the variables X_i and the interaction between X_iX_j, respectively. Interaction between factors was limited to only first order interactions (b_{ij}) due to this being able to represent the main effects without providing excessive degrees of freedom to the model. The model with the best fit was selected for each of the responses and operating conditions, maintaining the convention of using significant terms with $p < 0.05$ and r-squared above 80%, with and F-statistic that allows to reject the null hypothesis in each case.

$$Y = b_0 + \sum b_i X_i + \sum b_{ij} X_i X_j \qquad \text{Eq. 6}$$

Further information on the DOE and model evaluation can be seen in appendix 1.

3 Results

The current section is divided into three subsections. The first one corresponds to the effects of using the LCFs as drop-in alternatives for diesel, the second one is an evaluation of the combustion phasing; the emissions and fuel consumption potential the LCDs have when the same CA50 is maintained; and finally, an optimization of the operating conditions with equal combustion phasing is obtained to assess the potential a calibration aimed at reducing NOx has on the engine performance compared with conventional diesel combustion. As previously mentioned, experimental uncertainty is addressed by repetition of each measurement and the inclusion of the standard deviation between repetitions. Results hereby presented are shown in a way that intents to preserve the intellectual property of the OEM but allows to quantitatively evaluate the differences between fuels.

3.1 Baseline calibration combustion

Firstly, the fuels are evaluated using the baseline calibration provided by the OEM, thus serving to assess the drop-in capabilities of the fuels without modifying existing calibrations. Drop-in tests are intersting as they represent the most likely scenario for the future use of renewable fuels. These tests verify if a fuel is compatible with existing infrastructure without requiring any changes to the engine or the calibration settings. Ensuring a fuel is apt to be a drop-in alternative could prevent, in the scenario where the fuel is made commercially widespread, the need to recall fleets of circulating vehicles to perform changes in the calibration or hardware (which is a process that could take considerable time and resources). In that sense, for the current tests under the baseline diesel B7 calibration, the pedal position is varied to increase the fuel mass injected in the engine and reach the target load. As the fuels have different energy densities, the pedal position varies to compensate the energy deficiency for the fuels with lower LHV (around 1.7%). With the fuel demand indicated, the other calibration parameters are adjusted based on calibration maps with lookup values based on the engine speed and fuel mass, and finer adjustments are made based on a feedback loop with the actuators' sensors (temperatures, pressures, and flow).

3.1.1 Combustion characteristics

Figure 3 shows the heat release rate (HRR) vs the crank angle degree for the combustion of LCD100, LCD66 and LCD33 at 14 bar BMEP and 1500 rpm (for brevity only this operating condition is described in the body of the text, however the other operating conditions can be found in the appendix). These results were calculated using an in-house software called Calmec [42]. Additionally, the figure shows the absolute differences in calibration settings between the different fuels. From the calibration settings, the SOI and injection pressure for LCD100 and LCD33 are very similar, but in the case of the LCD66 the injection is advanced with respect to the other fuels by 0.15 CAD while the injection pressure is reduced by 25 bar (which for reference represents only around 3% of the mean rail pressure for all fuels). The other noticeable differences among the different fuel calibrations correspond to the air mass per stroke and the boost pressure, nonetheless the maximum differences between these values correspond to 1% and 3% respectively. These small settings variations are due to the similar lower heating values between the three fuels, which makes the operation maps coincidental for all three cases. The exception to this, however, is the EGR level in the case of LCD33 which is constantly lower than for the other two fuels due to the lower oxygen content in the fuel composition and the necessity to operate with a leaner mixture to reduce the sooting potential. In the HRR, it is observed that the fuels with higher cetane indexes exhibit higher low temperature heat release (LTHR) and the fuels with higher oxygen content also present a lower ignition delay of the pilot injection. In terms of the HRR peak, the behaviors for LCD66 and LCD33 are similar, while it can be said for the case of LCD100 that the slightly lower peak and lower tail are a consequence of the higher oxygen content and lower LHV in the fuel promoting shorter, less energetic combustion.

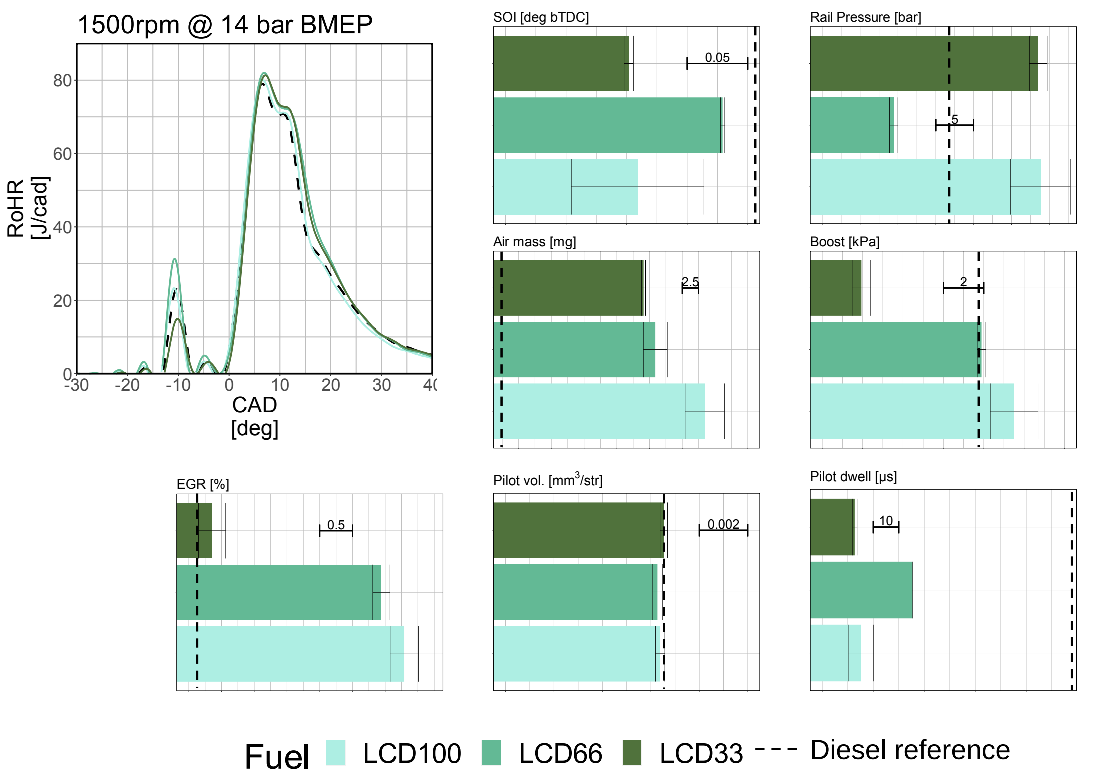

Figure 3. Effect of different LCF combustion on heat release rate with the baseline calibration for the operating condition 1500 rpm @ 14 bar.

To assess the combustion phasing each of the fuel blends, the CA50 and the combustion duration are used as indicators. In the current work, the combustion duration is defined as the difference between the CA10 (crank angle degree where 10% of the HRR accumulated has occurred) and the CA90 (crank angle degree where 90% of the accumulated HRR has occurred). Figure 4 shows how at higher loads the combustion is delayed for LCD33 due to its lower cetane index, in addition to this, the higher oxygen proportion in the LCD66 and LCD100 advances their combustion with respect to LCD33. Similar results were found in tests with the oxygen content in biodiesel compared to diesel in [43]. At lower loads, the effect of the different fuels is not as evident due to the proportionally higher EGR quantities which define the combustion phasing. Regarding the combustion duration, it can be generalized that the LCD33 has a shorter duration due in part to its shorter start of combustion (SOC) delay, and generally lower EGR proportion that facilitates a sooner end of combustion. The outlying longer combustion duration evident for the LCD66 fuel blend at the operating condition 2000 rpm @ 8 bar is a consequence of a vastly different calibration that uses three injections instead of two (in the case of LCD100 and LCD33) so the SOC occurs earlier as the pilot injections ignite faster.

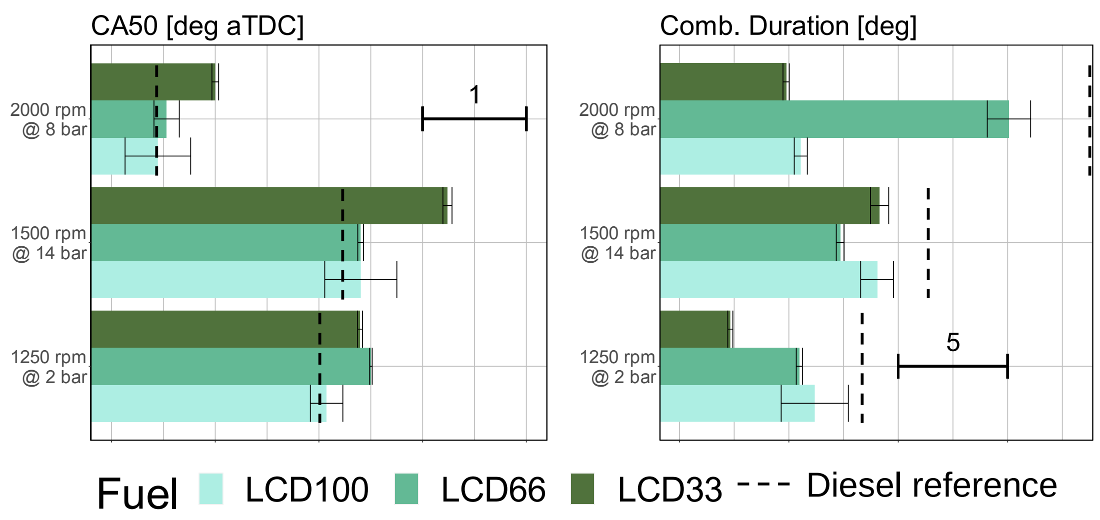

Figure 4. Combustion phasing [left] CA50 [right] combustion duration with the baseline calibration.

3.1.2 Engine performance and emissions

The brake specific fuel consumption (BSFC) in both equivalent and non-equivalent terms for the drop-in assessment of the fuels is reflected on Figure 5. The three LCF are compared with a diesel reference, and it can be noted that all fuels have a higher fuel consumption due to their reduced LHV. Additionally, the BSFC is for the operating conditions 1250 rpm @ 2 bar and 2000 rpm @ 8 bar the follows the expected trend where the fuel with the higher LHV has a lower fuel consumption. In the case of the 1500 rpm @ 14 bar, the fuel consumption is less dependent on the LHV as the operating condition has a higher load and is highly benefited by the oxygen present in the fuel to promote a better burning inside the cylinder. Assessing the $BSFC_{eq}$ also shows how the fuels with higher oxygen proportions (coming from the OMEx) improve the efficacy by which the fuels' energy is converted into useful work. In this regard it is also worth noticing how for most operating conditions the LCF blends perform better than the diesel reference in terms of $BSFC_{eq}$.

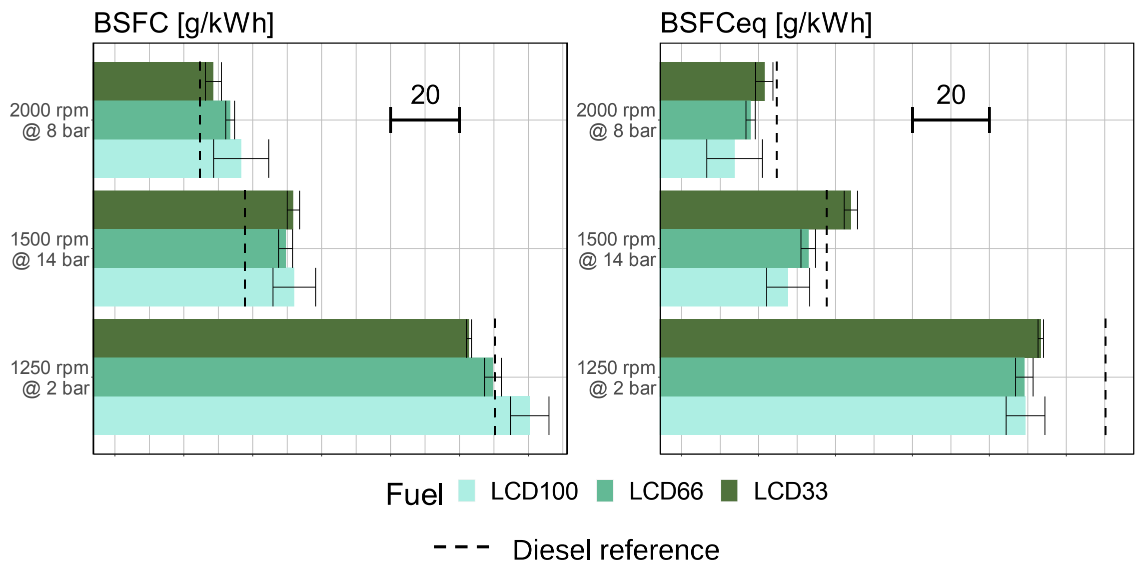

Figure 5. Fuel consumption for the LCF as drop-in candidates [left] BSFC [right] $BSFC_{eq}$.

Regulated emissions are also evaluated under the framework of using the LCF blends as drop-in alternatives. Figure 6 displays the criteria pollutant emissions that can be obtained with the evaluated LCFs using the engine's baseline calibration. The fuels with higher OMEx show higher NOx emissions due to the higher temperature and longer combustion durations that propitiate NOx formation. Nonetheless, when compared to reference diesel emissions most LCFs show lower emissions for all tested operating conditions emissions. Differences in soot emissions between the tested LCFs are below 0.05 g/kWh (in the worst-case scenario) and remain lower than the reference diesel case for all operating conditions. This is attributed to the fact that oxygen in the fuel eases the reduction of soot emissions. HC emissions for both LCD100 and LCD66 are similar, while LCD33 has emissions at least 0.2 g/kWh higher at medium and high load. Finally, it should be commented that CO remains close to the reference diesel values with the exception of the LCD33 under the 1500 rpm and 14 bar condition, where the elevated CO emissions indicate incomplete combustion of the fuel under the current calibration, which is not the case when the fuels have higher oxygen proportions.

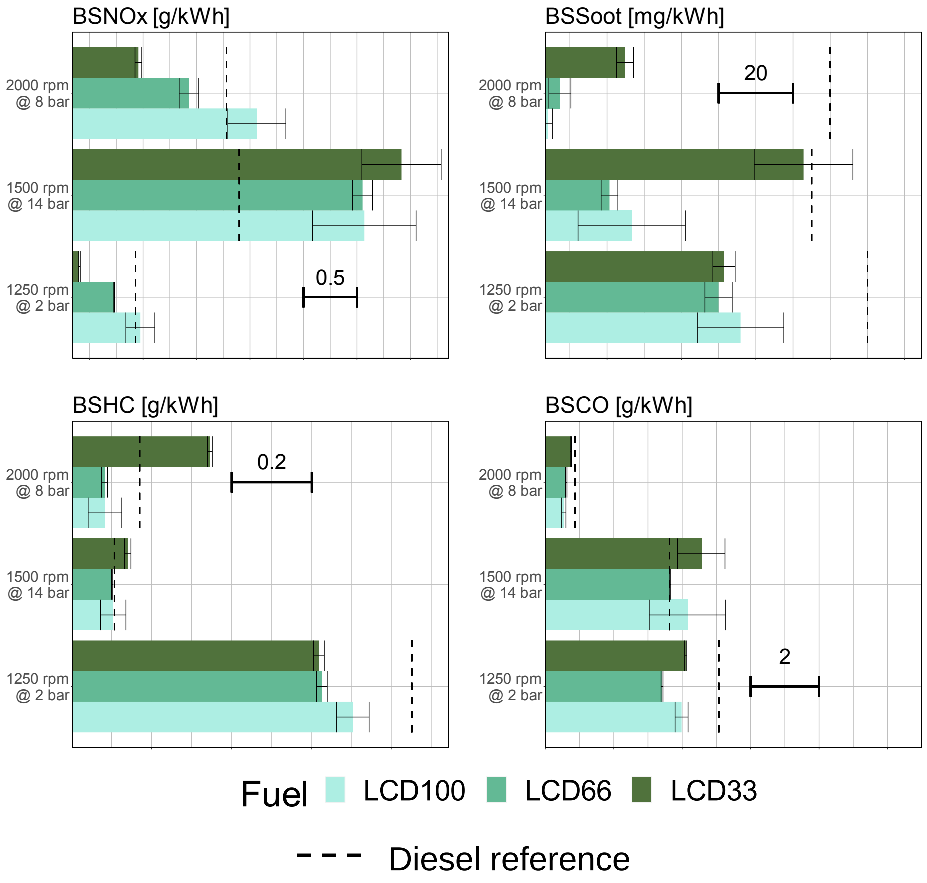

Figure 6. Criteria pollutants emissions for the LCF as drop-in candidates [top-left] BSNOx [top-right] BSSoot [bottom-left] BSHC [bottom-right] BSCO.

As the final step in the LCF evaluation as drop-in candidates the CO_2 emissions were calculated in WTT, TTW -or tailpipe CO_2 emissions-, and WTW. With the results shown in Figure 7, the potential for the LCF to mitigate CO_2 emissions is evident, in all three fuel lifecycle scenarios the amount of renewable content in the blend is directly proportional to the reduction in CO_2 emissions. Particularly, in WTT emissions a CO_2 offset of more than 500 g/kWh can be generated. Additionally, with the LCF blends it is possible to achieve reductions of up to 100 g/kWh in TTW emissions at low loads and speeds. The effects in WTT and TTW are compounded in the WTW emissions making it possible for the LCD100 to have reductions in CO_2 that are on average 961 g/kWh lower than the reference diesel combustion.

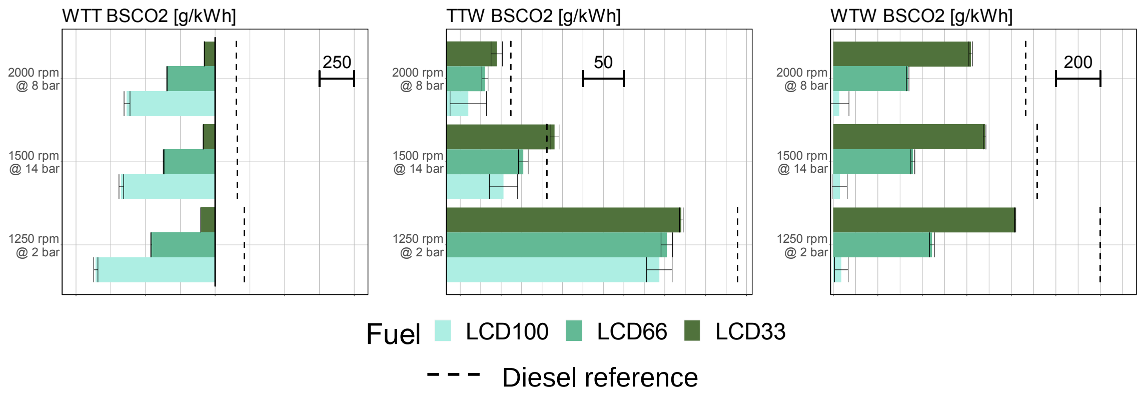

Figure 7. CO_2 emissions for the LCF as drop-in candidates [left] WTT $BSCO_2$ [middle] TTW $BSCO_2$ [right] WTW $BSCO_2$.

3.2 Effect of the LCF on the combustion under equal combustion phasing

The models described in section 2.3 are used to sample the distribution of the combustion phasing within the constraints imposed for emissions and engine safety parameters. As has been previously demonstrated the SOI has an important effect in the combustion phasing in compression ignition engines [44], for that reason the SOI was fixed to the average value between the three LCFs for each operating condition in the drop-in tests, which results in a SOI that is between the maximum and minimum observed for each engine condition across all LCFs. Regarding the injected fuel mass, the total amount is maintained equal to the fuel mass injected in the drop-in tests for each operating condition and LCF. Additionally, to guarantee a fair comparison between fuels, each parameter maximum and minimum limits (rail pressure, fresh air mass quantities, boost pressure and pilot injections) are made equal and emission constraints imposed for soot and NOx are respected. As observed in Figure 8, for the lower loads the median combustion phasing is more advanced for the fuels with higher OMEx quantities as the effect of the cetane index and the oxygen composition reduce the ignition delay. For the higher load, the trend is inversed. This is mainly due to EGR quantities needing to be reduced (and the air mass increased) to avoid the soot with the less oxygenated fuels; in turn, the fuels with higher oxygen possibly generate over-lean areas that could potentially delay the combustion. To expand on this idea, the evaluation of the median CA50 for the subdivision of cases with the same intake air mass quantity at the 1500 rpm @ 14 bar operating condition was performed, showing that the variation of the CA50 across the three fuels is less than 0.4 CAD. The previous fact could support the argument that at that load and speed the combustion phasing is more dependent on the air mass quantity than the cetane index and oxygen content in the fuel, as by removing the variation of one factor the effect size is significantly reduced.

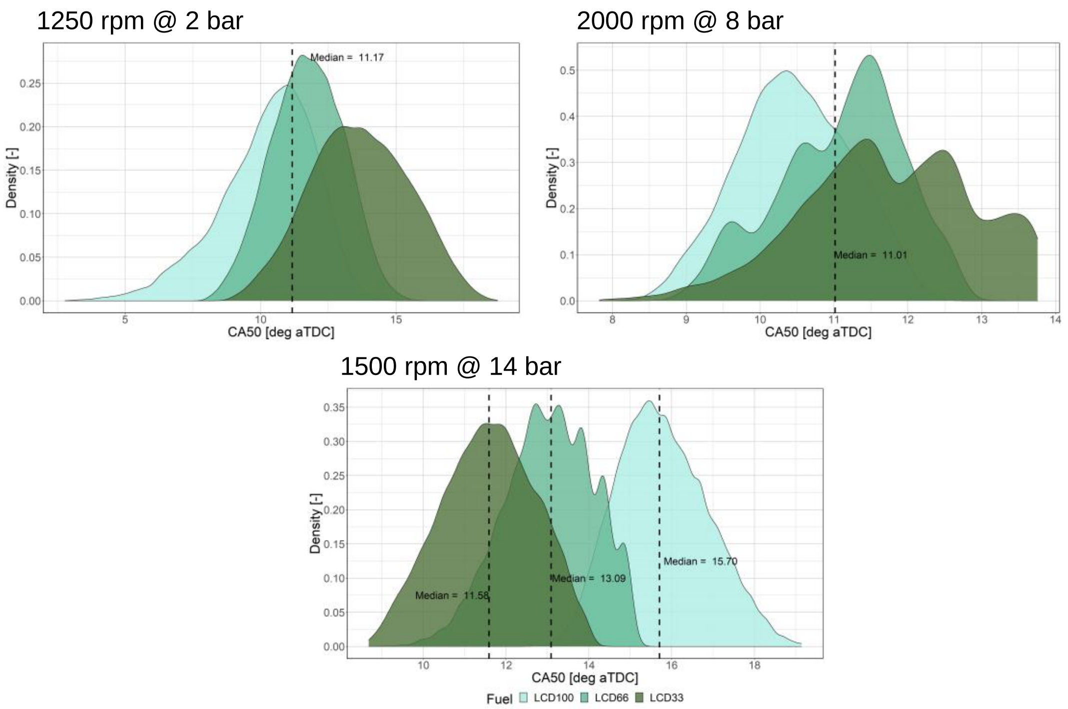

Figure 8. CA50 density distribution for the operating conditions [top-left] 1250 rpm @ 2 bar [top-right] 2000 rpm @ 8 bar [bottom] 1500 rpm @ 14 bar.

The potential responses of interest were evaluated using the same CA50, as can be seen in Figure 9 to 11. The modelled spaces show the tradeoff between BSNOx, BSFC and GBE. In all the tested operating conditions, the fuel consumption trends are strongly defined by the LHV of the fuel blend, with the median value of BSFC being higher as the fuel is less energy dense. In the high and low load cases, the GBE is higher in the case of LCD100 as its higher oxygen content aids the fuel conversion. NOx emissions show a homogeneous behavior across LCFs and operating conditions, with a slight increase as the fuel has less OMEx. It should be reminded in this regard that the modelled space is limited in the maximum amount of NOx that can be reached, thus the maximum possible NOx emissions with each fuel cannot be observed. Regarding soot emissions, it is evident how the higher proportion of oxygen content in the fuel and higher cetane number contribute to the reduction of this pollutant. The case of operating condition 2000 rpm @ 8 bar shows a small modification in the efficiency trends as the LCD66 has the highest efficiency of the fuels tested and fuel consumption is similar to that of LCD33.

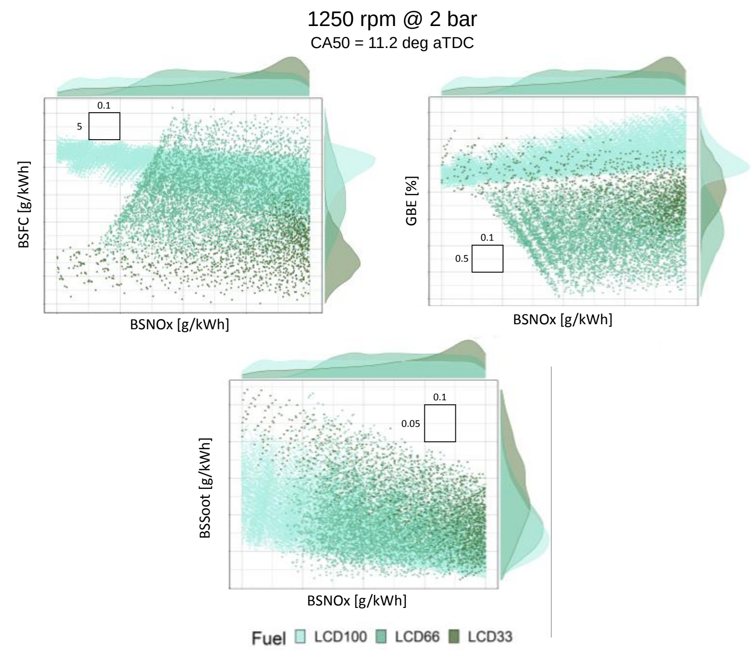

Figure 9. 1250 rpm @ 2 bar: fuel consumption, emissions, and efficiency potential with the same CA50. [top-left] BSFC vs. BSNOx [top-right] GBE vs. BSNOx [bottom] BSSoot vs. BSNOx.

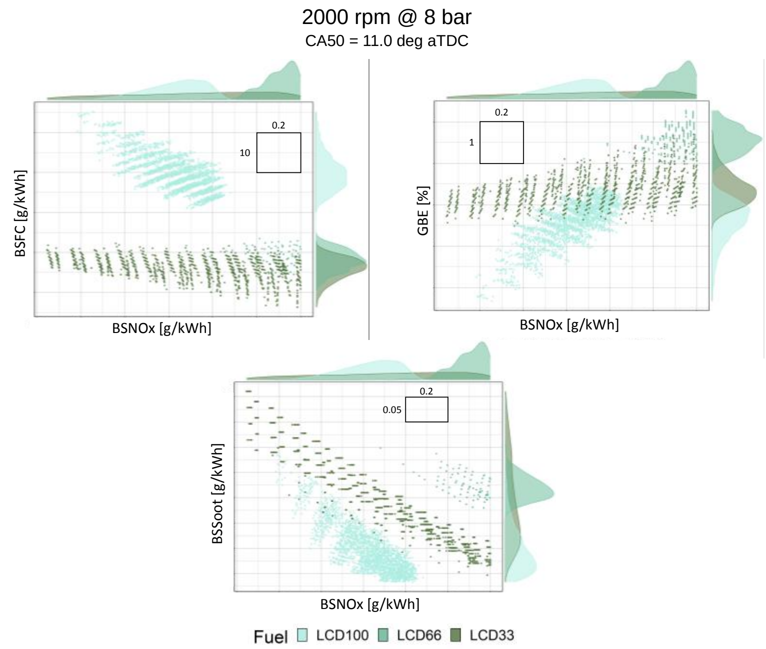

Figure 10. 2000 rpm @ 8 bar: fuel consumption, emissions, and efficiency potential with the same CA50. [top-left] BSFC vs. BSNOx [top-right] GBE vs. BSNOx [bottom] BSSoot vs. BSNOx.

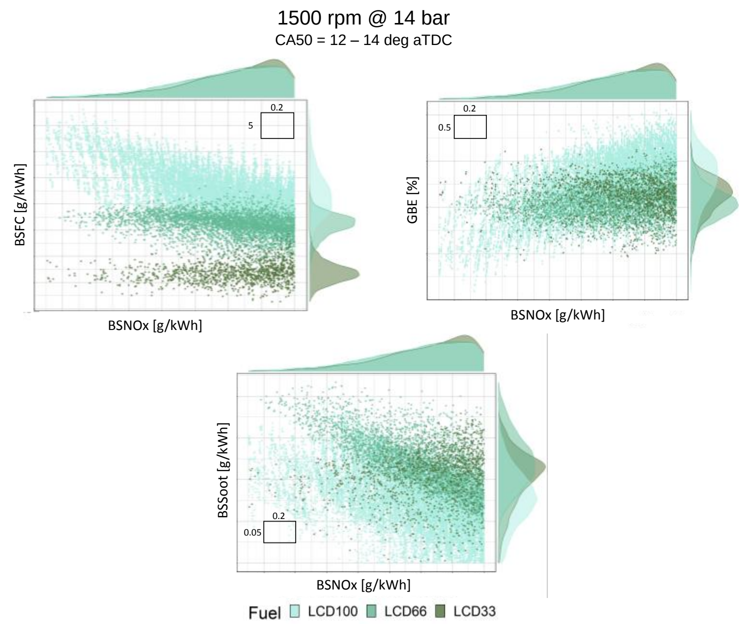

Figure 11. 1500 rpm @ 14 bar: fuel consumption, emissions, and efficiency potential with the same CA50. [top-left] BSFC vs. BSNOx [top-right] GBE vs. BSNOx [bottom] BSSoot vs. BSNOx.

Across the modelled spaces, the trends for the median value of the different responses of interest are shown in Figure 12 in a more synthetized form. The fuel consumption has an average increase of 1.93 g/kWh for every 1% v/v the fuel has in OMEx. In relation to the GBE, it cannot be said the OMEx proportion has significative effect within the specified parameters. Something similar can be said about NOx emissions as the rate of decrease for every 1% v/v of OMEx more in the blend does not exceed 0.012 g/kWh. Soot emissions, on the other hand, can be reduced up to 48.6% when going from a fuel with 5% OMEx concentration in volume to 15%.

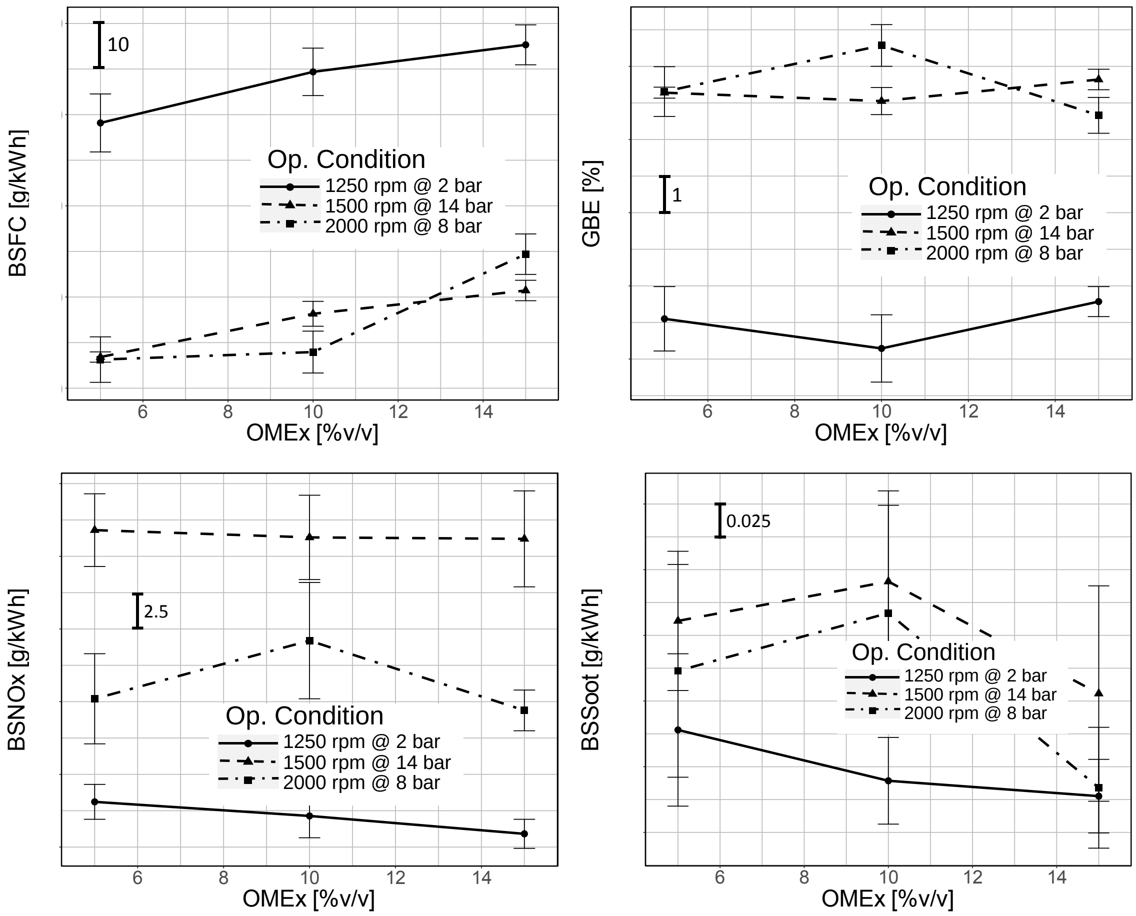

Figure 12. Median modelled space values for the different responses of interest vs. the proportion of OMEx present in the fuel [top-left] BSFC [top-right] GBE [bottom-left] BSNOx [bottom-right] BSSoot.

3.3 Optimization of LCF with equal CA50

Considering the defined modelled spaces, an optimization of the operating condition towards low NOx emissions (under 1 g/kWh for the 1250 rpm @ 2 bar condition, 2 g/kWh for the 2000 rpm @ 8 bar one and 3 g/kWh for the 1500 rpm @ 14 bar condition), and the lowest possible soot and fuel consumption values is attempted and experimentally measured. The optimization methodology is defined by equations 5 to 8, where ϵ is the admissible threshold for the desired responses. Only one calibration is selected for each operating condition and fuel. The new calibration parameters are shown in Table 5, compared to the baseline ECU calibration for each fuel and operating condition. In that regard, the parameters with the biggest differences between calibrations are the injection pressure, the intake air mas and the pilot injection volume and dwell times. Nonetheless as the effect of the different parameters is intrinsically correlated, the only defined trend is the reduction of the fresh air intake mass to reduce the EGR proportion in the mix and thus reduce the NOx emissions.

$$\mathrm{BSNOx} < \mathrm{BSNOx}_{min}(1+\epsilon) \qquad \text{Eq. 5}$$

$$\mathrm{BSSoot} < \mathrm{BSSoot}_{min}(1+1.2\epsilon) \qquad \text{Eq. 6}$$

$$\mathrm{BSFC} < \mathrm{BSFC}_{min}(1+2\epsilon) \qquad \text{Eq. 7}$$

$$\mathrm{GBE} > \mathrm{GBE}_{max}(1-2\epsilon) \qquad \text{Eq. 8}$$

Table 5. Optimized calibration parameters compared to the baseline calibration. Positive values indicate an increase of the parameter and negative values indicate a reduction.

		New Calibration - Baseline Calibration							
		SOI [deg bTDC]	Rail press. [bar]	Air mass [mg/st]	Boost press. [kPa]	Pilot vol. 1 [mm3]	Pilot dwell 1 [µs]	Pilot vol. 2 [mm3]	Pilot dwell 2 [µs]
1250 rpm @ 2 bar	LCD 100	0.78	-15.9	-112.8	-1.9	0.4	0.0	-0.40	0.44
	LCD 66	0.64	56.3	-71.5	-4.6	-0.5	0.0	0.00	50.30

	LCD 33	2.29	40.3	-87.4	-2.5	0.2	0.0	0.00	-9.72
2000 rpm @ 8 bar	LCD 100	-0.14	-0.7	-71.8	5.9	-0.2	605.5	-	-
	LCD 66	-0.49	-157.7	-71.5	-8.0	0.0	58.6	1.84	-200
	LCD 33	-1.47	257.8	-60.3	-4.4	0.9	212.0	-	-
1500 rpm @ 14 bar	LCD 100	-0.11	111.2	-58.4	-0.2	3.2	-465.2	-	-
	LCD 66	-0.18	-119.4	-60.9	-10.9	0.7	-35.4	-	-
	LCD 33	-0.10	-88.5	-44.1	-7.9	1.2	-562.7	-	-

The optimum calibration is tested in the engine by fixing the same fuel mass as the baseline calibration and defining in the ECU each of the model-determined parameters. The experimentally measured optimum points were compared to the modelled conditions, resulting in a maximum difference of 9.7% between experimental and modelled results(value obtained for the soot emissions), the rests of the differences between modelled and experimental values do not exceed 5%.

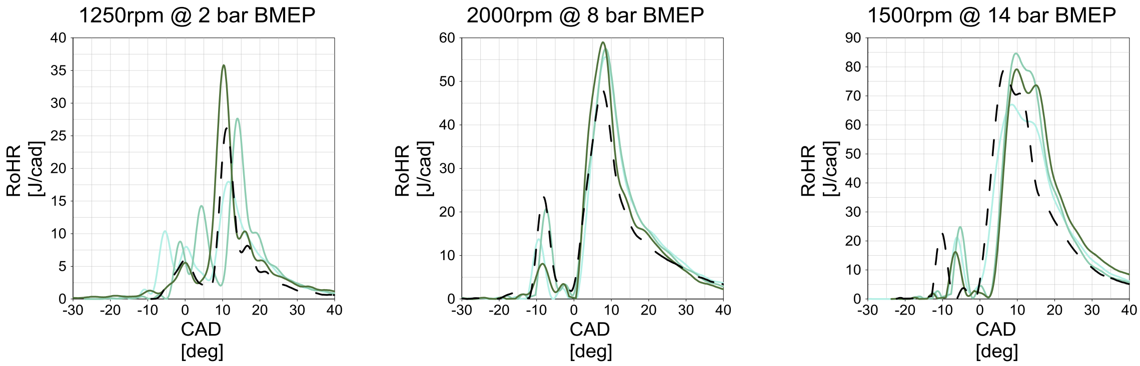

Figure 13. Effect of different LCF combustion on heat release rate with the optimized calibration

Although the CA50 is the same between LCFs, when optimizing the calibration, differences were observed in combustion start, combustion duration and peak heat release rate. In the case of the 1250rpm @ 2 bar operating condition, the advanced injections and increased injection pressures promote a bigger and more advanced LTHR and the combustion duration is extended with respect to the drop-in calibration. The 2000rpm @ 8 bar condition HRR shows very minor differences in comparison to the baseline calibration, although the start of the combustion is delayed 0.3 CAD as well as the end of the combustion for the LCFs. In addition, the peak of the HRR is slightly increased for the LCD100 and LCD66, and slightly decreased for the LCD33. Finally, the biggest differences are observed for the 1500rpm @ 14 bar operating condition due to the delayed injection, in conjunction with decreased injection pressures and increased EGR delay the start of the combustion by 3 CAD and the combustion duration is extended. It can also be observed for the LCD100 fuel a lower peak of the HRR, which by observing the variation in the parameters is likely caused by the increased of the injection pressure that causes the creation of zones with over rich air-fuel mixture (particularly near crevices) and will promote higher proportions of incomplete combustion, which will be noticed in the high CO emissions.

In Figure 14 it is observed how for the higher load operating conditions the BSFC is approximately 55 g/kWh higher with LCD100 than the diesel reference, while the other fuels also slightly increased their fuel consumption, as can be verified by the fact that $BSFC_{eq}$ is also higher than the diesel reference. This higher fuel mass required for the operation is due to the NOx reduction strategy that has a significantly higher EGR concentration that reduces fuel conversion efficiency. Fuel consumption optimization can be likely achieved with a dedicated calibration with the current LCFs, nonetheless there will likely be a tradeoff with NOx emissions as the emissions would be similar or higher to those of the drop-in tests. Another strategy could be to optimize the spray and flow conditions. Fuels with higher OMEx ratios require longer injections to provide the same energy as the baseline diesel fuel; in addition, the fuel tends to also burn faster [45]. Thus, there might be some potential for further optimization of fuel efficiency by changing the injectors for ones with a higher flowrate (where shorter injections are possible with reduced injection pressures) and performing an optimization with similar emission reduction targets. Conversely, OMEx has a higher vapor pressure and thus a lower liquid penetration length [46], and it has been previously shown that injectors with bigger diameter can increase the spray penetration of OMEx and cause a longer ignition delay [47], these characteristics could contribute in achieving lean-burn conditions for OMEx that improve fuel consumption, similarly to the lambda variations performed in [17]. Nonetheless, further research is needed to verify this hypothesis.

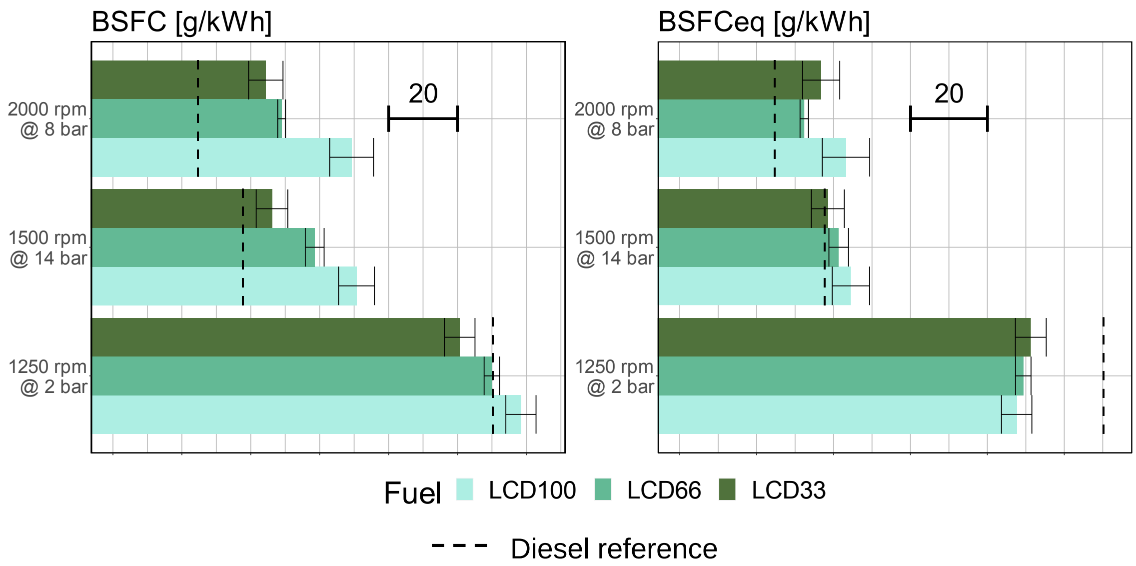

Figure 14. Fuel consumption for the optimized calibration of LCF [left] BSFC [right] $BSFC_{eq}$.

The calibration optimization in most operating conditions and fuels is able to reduce BSNOx emissions by 1 g/kWh (Figure 15), compared to the diesel reference. This reduction in BSNOx emissions comes to the detriment of soot emissions which are equal or higher than those of diesel for the higher load cases. Nonetheless, it is important to be reminded that the soot emissions correspond to engine-out emissions before the aftertreatment system, and that the vehicles which employ this engine integrate a diesel particulate filter to their system, which could potentially remove most soot particles with reliable efficiency. Conversely, although HC and CO emissions can be higher than diesel's with the calibration optimized for NOx reduction these emissions could be oxidized by the diesel oxidation catalyst (DOC), as shown in previous work [37]. Nonetheless, further testing is needed in this regard to evaluate whether an increase of CO of more than 10 g/kWh in the worst-case scenario can be addressed by the aftertreatment system. Additionally, different calibration targets can be explored to reduce emissions of both CO and HC emissions.

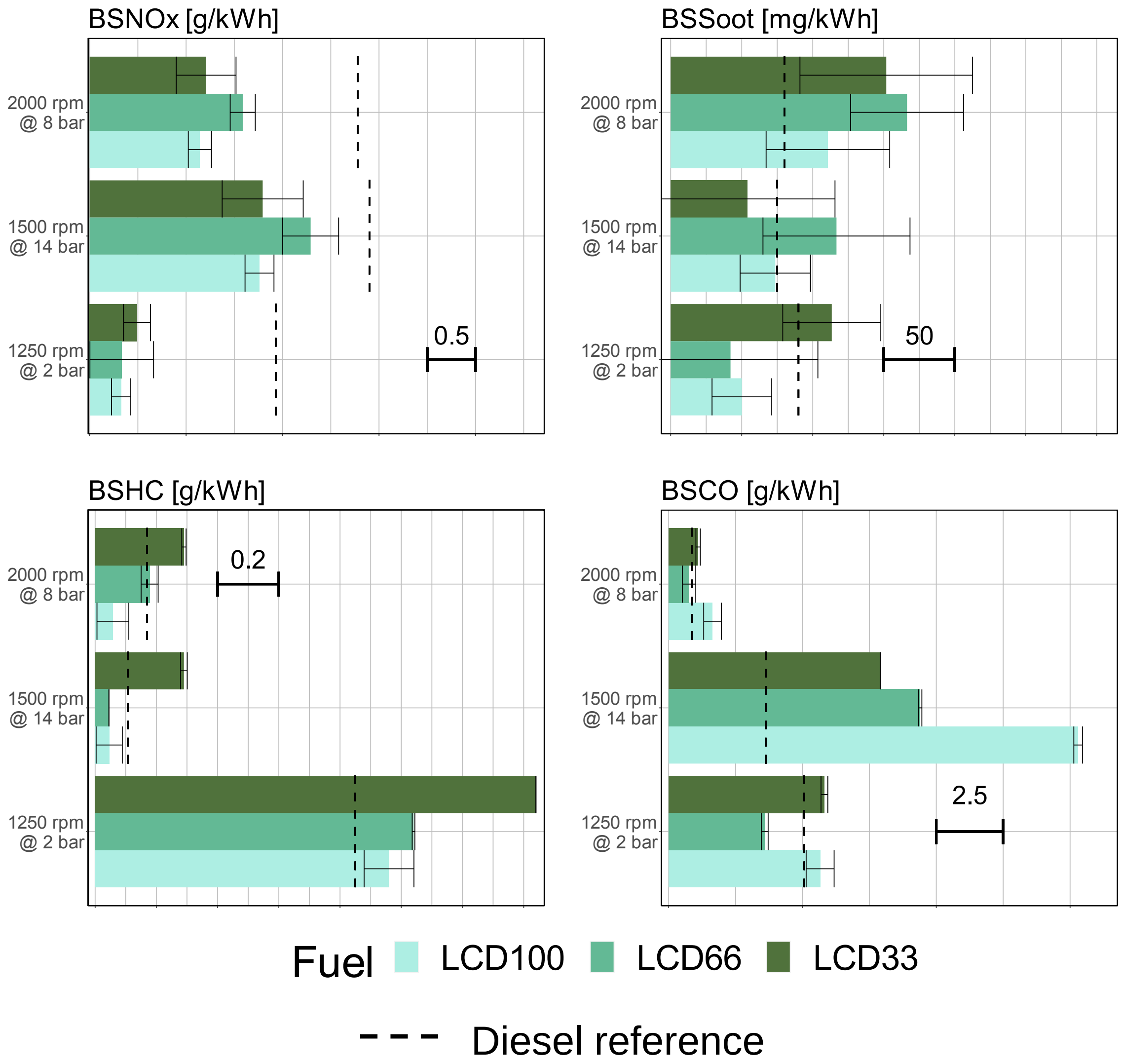

Figure 15 Criteria pollutants emissions for the optimized calibration of LCF [top-left] BSNOx [top-right] BSSoot [bottom-left] BSHC [bottom-right] BSCO

Finally, the CO_2 lifecycle emissions are calculated for each of the operating conditions and LCF blend (Figure 16). Although the TTW CO_2 emissions are higher due to higher fuel consumption, they remain below those of diesel. Similarly to the drop-in results, the CO_2 offset generated by the fuel synthesis translates into WTW CO_2 emissions that are at least 200 g/kWh lower than the diesel reference for LCD33 and up to 1200 g/kWh lower for the completely renewable LCD100. In the specific case of LCD100, it can be noted that the differences in WTW BSO2 between both calibrations is smaller than the effect caused by the different operating conditions.

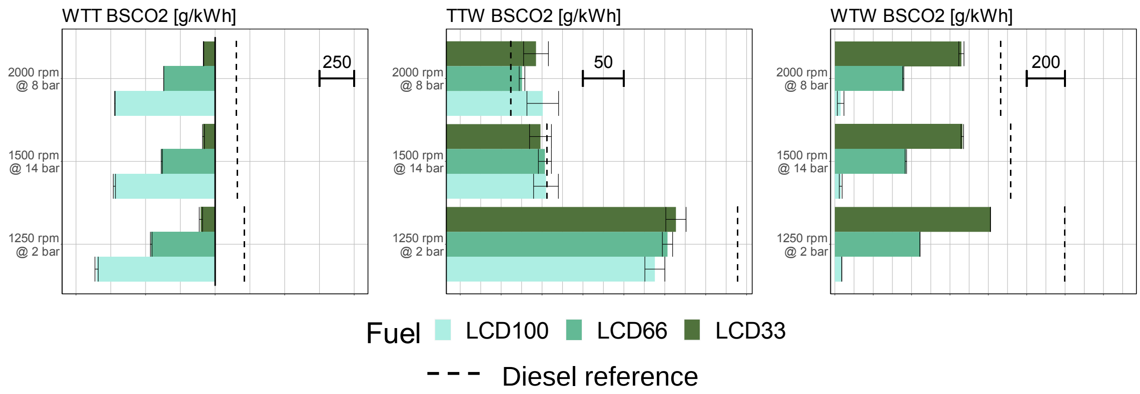

Figure 16. CO_2 emissions for the optimized calibration of LCF [left] WTT $BSCO_2$ [middle] TTW $BSCO_2$ [right] WTW $BSCO_2$.

4 Summary and conclusions

Three LCFs were studied and compared in terms of combustion performance and emissions under a baseline calibration. Subsequently, by means of a design of experiments, linear models were obtained that allowed the evaluation of the effect of the different LCF on the combustion phasing and the fuel consumption and emissions potential. Additionally, taking advantage of the resulting models a calibration optimization was performed and later verified experimentally with the objective of reducing NOx emissions, while maintaining the lowest possible soot emissions and fuel consumption and the highest efficiency. The current section summarizes the most relevant findings of the work.

- When comparing to diesel, using LCFs with varying proportions of OMEx under the baseline ECU calibration decreases soot emissions by at least 5 mg/kWh, while increasing fuel consumption due to the lower LHV. . There is not a direct correlation with NOx emissions, which can either be lower or higher than the diesel reference depending on the engine load.
- For the lower load operating conditions, the combustion phasing of the LCFs varies depending mostly on the cetane index of the fuel and the oxygen content of the blend. In this regard, a generally more advanced

combustion occurs in the case of LCD100. When the load is increased the trend is not observed due to the air mass quantity being a more determining factor in the combustion phasing.

- When the CA50 is equal across all LCFs, fuel consumption is generally higher and soot emissions are lower for the fuel with higher OMEx proportion (LCD100) due to its higher oxygen content that aids in the complete oxidation of the fuels but reduces its energetic density.
- When optimizing the LCFs' calibration for low NOx emissions, this pollutant can be reduced by at minimum 0.5 g/kWh compared to the reference diesel, however other pollutants such as PM, HC and CO can increase with respect to diesel. Future work could address the evaluation of the efficiency of the ATS at reducing the pollutant emissions of the optimized calibration.
- The use of LCF under both the baseline ECU calibration and the optimized calibration reduces the WTW $BSCO_2$ by 200 g/kWh for LCD33 (33% v/v renewable content) and by 1200 g/kWh for LCD100 (100% v/v renewable content). This reductions in CO_2 emissions show that a variation of 67% v/v in renewable content can generate an 83% difference in WTW CO_2 emissions.

Acknowledgments

The authors thank ARAMCO Overseas Company for supporting this research.

References

[1] A. Liberale Rispoli, N. Verdone and G. Vilardi, "Green fuel production by coupling plastic waste oxy-combustion and PtG technologies: Economic, energy, exergy and CO2-cycle analysis," *Fuel Processing Technology,* vol. 221, p. 106922, 2021.

[2] H. L. Chum and R. P. Overend, "Biomass and renewable fuels," *Fuel Processing Technology,* vol. 71, no. 1-3, pp. 187-195, 2001.

[3] A. Calle-Asensio, J. Hernández, J. Rodríguez-Fernández, M. Lapuerta, A. Ramos and J. Barba, "Effect of advanced biofuels on WLTC emissions of a Euro 6 diesel vehicle with SCR under different climatic conditions," *Int. J. Engine Res.,* 2021.

[4] L. Cai, S. Jacobs, R. Langer, F. vom Lehn, K. A. Heufer and Pitsch, "Auto-ignition of oxymethylene ethers (OMEn, n = 2–4) as promising synthetic e-fuels from renewable electricity: shock tube experiments and automatic mechanism generation," *Fuel,* vol. 264, no. March, p. 116711, 2020.

[5] D. Candelaresi and G. Spazzafumo, "1 - Introduction: the power-to-fuel concept," in *Power to Fuel, How to Speed Up a Hydrogen Economy*, 2021, pp. 1-15.

[6] L. Grégoire, L. Vincent, E. Damien, J. M. Christoph and S. L. Klaus, "Electricity storage with liquid fuels in a zone powered by 100% variable renewables," *12th International Conference on the European Energy Market (EEM),* pp. 1-5, 2015.

[7] H. Yangdong, L. Zhu, J. Fan, L. Li and G. Liu, "Life cycle assessment of CO2 emission reduction potential of carbon capture and utilization for liquid fuel and power cogeneration," *Fuel Processing Technology,* vol. 221, p. 106924, 2021.

[8] M. Mikulski, M. Ambrosewicz-Walacik, K. Duda and J. Hunicz, "Performance and emission characterization of a common-rail compression-ignition engine fuelled with ternary mixtures of rapeseed oil, pyrolytic oil and diesel," *Renew. Energy,* vol. 148, pp. 739-755, 2020.

[9] K. van Kranenburg, Y. van Delft, A. Gavrilova, R. de Kler, C. Schipper, R. Smokers, M. Verbeek and R. Verbeek, "E-fuels: towards a more sustainable future for truck transport, shipping and aviation," TNO VoltaChem Smartport, Delft, 2020.

[10] H. Bayraktar, "An experimental study on the performance parameters of an experimental CI engine fueled with diesel–methanol–dodecanol blends," *Fuel,* vol. 87, no. 2, pp. 158-164, 2008.

[11] O. James, A. M. Mesubi, T. C. Aki and S. MAity, "Increasing carbon utilization in Fischer–Tropsch synthesis using H2-deficient or CO2-rich syngas feeds," *Fuel Processing Technology,* vol. 91, no. 2, pp. 136-144, 2010.

[12] Y. Huang, S. Wang and L. Zhou, "Effects of Fischer-Tropsch diesel fuel on combustion and emissions of direct injection diesel engine," *Front. Energy Power Eng. China,* vol. 2, no. 3, pp. 261-267, 2008.

[13] F. Andrade Torres, O. Doustdar, J. Martin Herreros, R. Li, R. Poku, A. Tsolakis, J. Martins and S. A. B. Vieira de Melo, "A Comparative Study of Biofuels and Fischer–Tropsch Diesel Blends on the Engine Combustion Performance for Reducing Exhaust Gaseous and Particulate Emissions," *Energies,* vol. 14, p. 1538, 2021.

[14] A. Omari, B. Heuser and S. Pischinger, "Potential of oxymethylenether-diesel blends for ultra-low emission engines," *Fuel,* vol. 209, no. December 2017, pp. 232-237, 2017.

[15] A. García, J. Monsalve-Serrano, D. Villalta and M. Guzmán-Mendoza, "Methanol and OMEx as fuel candidates to fulfill the potential EURO VII emissions regulation under dual-mode dual-fuel combustion," *Fuel,* vol. 287, p. 119548, 2021.

[16] R. Sathiyamoorthi, G. Sankaranarayanan, M. Venkatraman, D. Babu Munuswamy and R. Ravisankar, "Environment-friendly fuel Cymbopogon flexuosus: Analysis of fuel properties, performance, and emission parameters of a Direct Injection Compression Ignition research engine," *Heat Transfer,* vol. 50, no. 7, pp. 6589-6627, 2021.

[17] A. García, J. V. D. Monsalve-Serrano and Á. Fogué-Robles, "Evaluating OMEx combustion towards stoichiometric conditions in a compression ignition engine," *Fuel,* vol. 303, p. 121273, 2021.

[18] A. García, J. Monsalve-Serrano, D. Villalta, R. Lago Sari, V. Gordillo Zavaleta and P. Gaillard, "Potential of e-fischer Tropsch diesel and oxymethyl-ether (OMEx) as fuels for the dual-mode dual-fuel concept," *Applied Energy,* vol. 253, p. 113622, 2019.

[19] J. Luján, A. García, J. Monsalve-Serrano, Martínez-Boggio and S., "Effectiveness of hybrid powertrains to reduce the fuel consumption and NOx emissions of a Euro 6d-temp diesel engine under real-life driving conditions," *Energy Conversion and Management,* vol. 199, p. 111987, 2019.

[20] IEA, "Net Zero by 2050," IEA, Paris, 2021.

[21] A. Ramirez, S. M. Sarathy and J. Gascon, "CO2 Derived E-Fuels: Research Trends, Misconceptions, and Future Directions," *Trends in Chemistry,* vol. 2, no. 9, pp. 785-795, 2020.

[22] N. O. Kapustin and D. A. Grushevenko, "Long-term electric vehicles outlook and their potential impact on electric grid," *Energy Policy,* vol. 137, p. 111103, 2020.

[23] R. García-Contreras, J. A. Soriano, P. Fernández-Yáñez, A. Gómez, O. Armas and M. Cárdenas, "Impact of regulated pollutant emissions of Euro 6d-Temp light-duty diesel vehicles under real driving conditions," *J. Clean. Prod.,* vol. 286, 2021.

[24] M. Williams and R. Minjares, "A technical summary of Euro 6/VIvehicle emission standards," icct - The International Council on Clean Transportation, 2016.

[25] E. Bannon, "Road to Zero: the last EU emission standard," *Transport & Environment,* pp. 1-19, 2020.

[26] S. Molina, A. García, J. Monsalve-Serrano and D. Estepa, "Miller cycle for improved efficiency, load range and emissions in a heavy-duty engine running under reactivity controlled compression ignition combustion," *Applied Thermal Engineering,* vol. 136, pp. 161-168, 2018.

[27] J. Monsalve-Serrano, G. Belgiorno, G. Di Blasio and M. Guzmán-Mendoza, "1D Simulation and Experimental Analysis on the Effects of the Injection Parameters in Methane–Diesel Dual-Fuel Combustion," *Energies,* vol. 13, no. 14, p. 3734, 2020.

[28] J. Wade and R. Farrauto, "12 - Controlling emissions of pollutants in urban areas," in *Metropolitan Sustainability: Understanding Improving the Urban Environment*, Woodhead Publishing Series in Energy, 2012, pp. 260-291.

[29] A. S. Ayodhya, Narayanappa and K. Gottekere, "An overview of after-treatment systems for diesel engines," *Environ Sci Pollut Res Int.,* vol. 25, no. 35, pp. 35034-35047, 2018.

[30] I. A. Reşitoğlu, K. Altinişik and A. Keskin, "The pollutant emissions from diesel-engine vehicles and exhaust aftertreatment systems," *Clean Technologies and Environmental Policy,* vol. 17, pp. 15-27, 2015.

[31] N. H., Y. Tanaka, T. Adachi, S. Kawamura, Y. Daisho, H. Suzuki and K. Yamaguchi, "A Study on the Improvement of NOx Reduction Efficiency for a Urea SCR System," *SAE Technical Paper,* Vols. 2015-01-2014, 2015.

[32] N. Singh, C. Rutland, D. Foster, K. Narayanaswamy and Y. He, "Investigation into Different DPF Regeneration Strategies Based on Fuel Economy Using Integrated System Simulation," *SAE Technical Paper,* Vols. 2009-01-1275, 2009.

[33] F. C. P. Leach, M. H. Davy and M. S. Peckham, "Cyclic NO2:NOx ratio from a diesel engine undergoing transient load steps," *Int. J. Engine Res.,* vol. 22, no. 1, pp. 284-294, 2021.

[34] V. Pedrozo, X. Wang, W. Guan and H. Zhao, "The effects of natural gas composition on conventional dual-fuel and reactivity-controlled compression ignition combustion in a heavy-duty diesel engine," *Int. J. Engine Res.,* 2021.

[35] L. Geng, L. Bi, Q. Li, H. Chen and Y. Xie, "Experimental study on spray characteristics, combustion stability, and emission performance of a CRDI diesel engine operated with biodiesel–ethanol blends," *Energy Reports,* vol. 7, no. November, pp. 904-915, 2021.

[36] M. Yugo, V. Gordillo, E. Shafiei and A. Megaritis, "A look into the life cycle assessment of passenger cars running on advanced fuels," in *SIA Powertrain & Electronics conference*, France, 2021.

[37] J. Benajes, A. García, J. Monsalve-Serrano and R. Sari, "Evaluating the Efficiency of a Conventional Diesel Oxidation Catalyst for Dual-Fuel RCCI Diesel Gasoline Combustion," *SAE Technical Paper,* vol. 01, no. Sept, p. 1729, 2018.

[38] R. Durrett and M. Potter, "Renewable Energy to Power through Net-Zero-Carbon Fuels," in *THIESEL 2020 Conference on Thermo- and Fluid Dynamic Processes in Direct Injection Engines 8th-11th September 2020*, Valencia, 2020.

[39] R. Sathiyamoorthi, G. Sankaranarayanan, M. Venkatraman, V. Jayaseelan and K. Sivakumar, "Analysis of optimising injection parameters and EGR for DICI engine performance powered by lemongrass oil using Box–Behnken (RSM) modelling," *International Journal of Ambient Energy,* 2022.

[40] D. C. Montgomery, Design and Analysis of Experiments, 10th Edition, New York: John Wiley, 2019.

[41] Analytical Methods Committee AMCTB No 55, "Experimental design and optimisation (4): Plackett–Burman designs," *Anal. Methods,* vol. 5, no. 8, pp. 1901-1903, 2013.

[42] F. Payri, P. Olmeda, J. Martin and R. Carreño, "A new tool to perform global energy balances in DI diesel engines," *SAE Int J Eng,* vol. 7, no. 1, pp. 43-59, 2014.

[43] R. Sathiyamoorthi, G. Sankaranarayanan, S. Adhith kumaar, T. Chiranjeevi and D. Dilip Kumar, "Experimental investigation on performance, combustion and emission characteristics of a single cylinder diesel engine fuelled by biodiesel derived from Cymbopogon Martinii," *Renewable Energy,* vol. 132, no. March, pp. 394-415, 2019.

[44] P. Mohamed Shameer, K. Ramesh, R. Sakthivel and R. Purnachandran, "Effects of fuel injection parameters on emission characteristics of diesel engines operating on various biodiesel: A review," *Renewable and Sustainable Energy Reviews,* vol. 67, pp. 1267-1287, 2017.

[45] A. García, J. Monsalve-Serrano, E. J. Sanchís and Á. Fogué-Robles, "Exploration of suitable injector configuration for dual-mode dual-fuel engine with diesel and OMEx as high reactivity fuels," *Fuel,* vol. 280, no. November, p. 118670, 2020.

[46] D. Goeb, M. Davidovic, L. Cail, P. Pancharia, M. Bode, S. Jacobs, J. Beeckmann, W. Willems, K. A. Heufer and H. Pitsch, "Oxymethylene ether – n-dodecane blend spray combustion: Experimental study and large-eddy simulations," *Proceedings of the Combustion Institute,* vol. 38, no. 2, pp. 3417-3425, 2021.

[47] J. V. Pastor, J. M. García-Oliver, C. Micó and A. A. García-Carrero, "An experimental study with renewable fuels using ECN Spray A and D nozzles," *International Journal of Engine Research,* no. July, pp. 1-12, 2021.

Abbreviations

BMEP	Brake mean effective pressure

CI	Compression ignition
DOC	Diesel oxidation catalyst
DOE	Design of experiments
DPF	Diesel particulate filter
EV	Electric vehicle
FAME	Fatty acid methyl esters
GBE	Gross brake efficiency
HC	hydrocarbons
HVO	Hydrogenated vegetable oil
ICE	Internal combustion engine
LCF	Low carbon fuel
LHV	Lower heating value
OEM	Original equipment manufacturer
PM	Particulate matter
PRR	Pressure rise rate
SI	Spark ignition
SOI	Start of injection
TTW	Tank-to-wheel
WLTC	World harmonized Light vehicle Test Cycle
WLTP	World harmonized Light vehicle Test Procedure
WTT	Well-to-tank
WTW	Well-to-wheel

Appendix

1 Model and design of experiments evaluation

The model factors to evaluate (SOI, injection pressure, pilot injection characteristics and air intake mass and pressure) were selected based on previous knowledge regarding engine responses to parametric changes in these values. The range size for each of the factors and operating conditions can be observed in Table 6. The ranges tested for each fuel and operating condition depend on parametric tests in which the maximum limit is found when the imposed emission limits or safety constraints (PRR and peak pressure) are close to borderline when increasing or decreasing the value. These preliminary tests also help in ensuring the effect of the variation of one factor is monotonous (increasing or decreasing), to be able to use a linear model.

Table 6. Factor ranges evaluation. Difference between maximum and minimum values evaluated during the DOE

Fuel	Operating condition	SOI [CAD]	Injection pressure [bar]	Pilot volume [mm^3]	Pilot dwell [µs]	Air mass [mg]	Boost pressure [kPa]
LCD100	1250 rpm @ 2 bar	5	100	3.5	275	70	5
	2000 rpm @ 8 bar	8	600	1.5	210	40	25
	1500 rpm @ 14 bar	5	450	4	800	50	10
LCD66	1250 rpm @ 2 bar	14	140	1.5	150	70	5
	2000 rpm @ 8 bar	20	700	4	600	60	20
	1500 rpm @ 14 bar	14	370	1.5	1000	30	10
LCD33	1250 rpm @ 2 bar	11	150	1.8	150	90	5
	2000 rpm @ 8 bar	5	500	2	400	50	10
	1500 rpm @ 14 bar	12	300	3	950	30	10

The effects size of each of the parameters under each operating condition and LCF was evaluated with the standardized effect. For brevity, Figure 17 only shows the effect for BSNOx, however a similar procedure was performed for all responses of interest. This results aid in providing an idea during the DOE and modelling phases of which factors are the most influential in the size of the responses.

Figure 17. Standardized effect for the BSNOx emissions

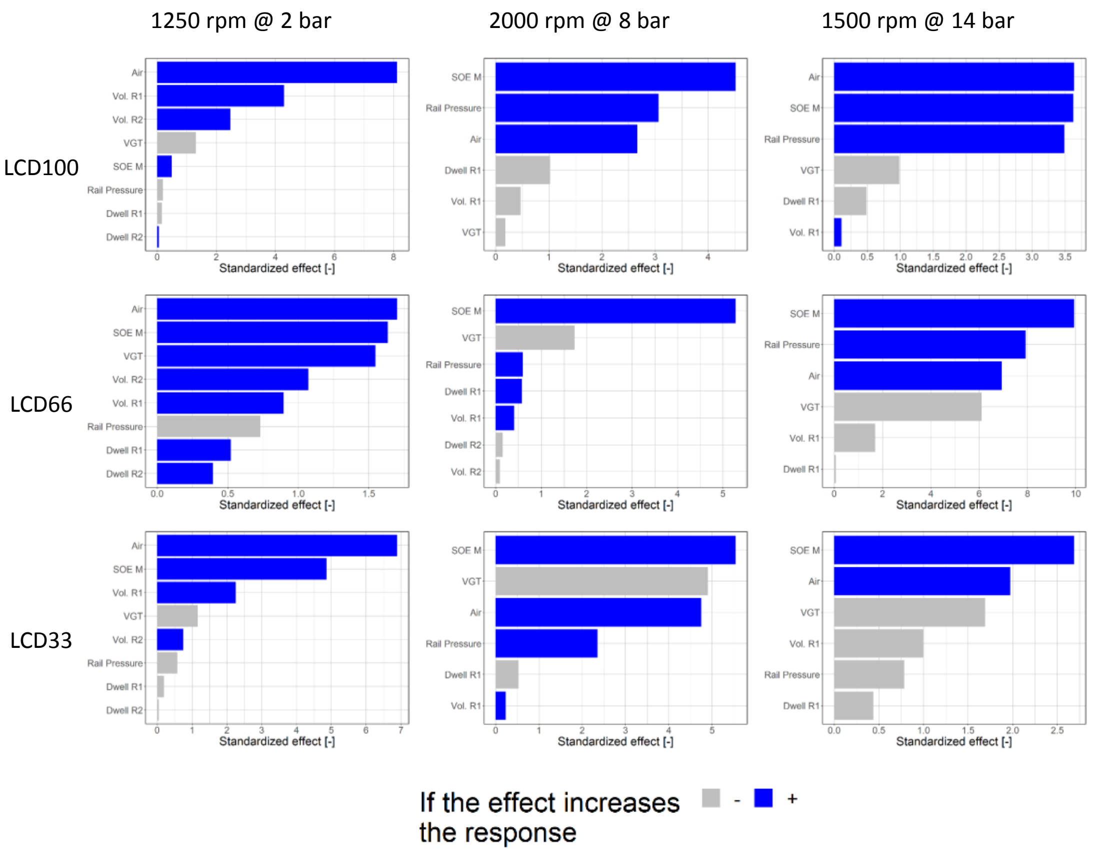

The model evaluation for the five main responses of interest can be seen in Table 7. The mean value is not expressed to maintain the OEM's proprietary information, however the fit of the model and the errors associated are described.

Table 7. Model evaluation parameters. Residual Standard Error (RSE), Degrees of Freedom (DF), R-squared (R2), F-Statistic, p-value.

Fuel		LCD 100			LCD66			LCD33		
Operating condition		1250 rpm @ 2 bar	2000 rpm @ 8 bar	1500 rpm @ 14 bar	1250 rpm @ 2 bar	2000 rpm @ 8 bar	1500 rpm @ 14 bar	1250 rpm @ 2 bar	2000 rpm @ 8 bar	1500 rpm @ 14 bar
GBE	RSE [%]	0.41	0.46	0.28	0.49	0.57	0.90	0.88	0.68	0.47
	DF	55	59	29	55	59	32	54	60	32
	R^2	0.876	0.875	0.947	0.920	0.898	0.888	0.961	0.847	0.813
	F-statistic	55.38	58.83	73.49	63.47	64.69	40.02	121.3	47.5	26.7

	p-value	2.2e-16	2.2e-16	2.2e-16	2.2e-16	2.2e-16	2.2e-16	2.2e-16	2.2e-16	7.1e-14
BSFC	RSE [g/kWh]	4.38	3.21	2.24	5.20	4.59	2.73	7.36	4.99	3.42
	DF	55	56	30	53	60	32	53	61	31
	R^2	0.874	0.889	0.934	0.920	0.873	0.885	0.820	0.844	0.804
	F-statistic	54.57	56.11	70.42	50.86	58.87	40.13	24.86	47.09	26.33
	p-value	2.2e-16	2.2e-16	2.5e-16	2.2e-16	2.2e-16	2.2e-16	2.4e-15	2.2e-16	1.7e-13
BSNOx	RSE [g/kWh]	0.096	0.138	0.326	0.154	0.425	0.290	0.124	0.244	0.279
	DF	52	55	27	53	50	31	55	60	32
	R^2	0.992	0.977	0.926	0.976	0.869	0.915	0.954	0.967	0.914
	F-statistic	632.7	257.3	37.38	177.3	92.11	69.73	114.4	252.5	73.15
	p-value	2.2e-16	2.2e-16	5.9e-13	2.2e-16	2.6e-15	2.2e-16	2.2e-16	2.2e-16	2.2e-16
BSSoot	RSE [g/kWh]	0.028	0.026	0.082	0.033	0.082	0.069	0.058	0.071	0.082
	DF	49	52	29	53	59	29	56	60	29
	R^2	0.854	0.912	0.809	0.829	0.846	0.804	0.827	0.863	0.802
	F-statistic	41.98	44.78	37.53	31.47	40.38	23.23	26.56	54.11	25.55
	p-value	4.6e-16	2.2e-16	7.4e-9	3.3e-16	2.2e-16	3.3e-16	7.4e-14	2.2e-16	2.8e-13
CA50	RSE [CAD]	0.296	0.093	0.304	0.436	0.471	0.431	1.79	1.14	0.526
	DF	47	55	32	56	62	32	58	65	32
	R^2	0.995	0.9998	0.988	0.996	0.998	0.992	0.944	0.980	0.987
	F-statistic	644	2.77e+4	633.1	1630	5566	3545	139.3	1626	2470
	p-value	2.2e-16	2.2e-16	2.2e-16	2.2e-16	2.2e-16	2.2e-16	2.2e-16	2.2e-16	2.2e-16

Finally, the model validation for the current manuscript is reflected in the experimentally measured optimum condition, whose values for the responses of interest are compared with the modelled results. Table 8 shows the error associated to the predictions from the models.

Table 8. Error between modelled and experimental responses

Fuel	LCD 100			LCD66			LCD33		
Operating condition	1250 rpm @ 2 bar	2000 rpm @ 8 bar	1500 rpm @ 14 bar	1250 rpm @ 2 bar	2000 rpm @ 8 bar	1500 rpm @ 14 bar	1250 rpm @ 2 bar	2000 rpm @ 8 bar	1500 rpm @ 14 bar
GBE [%]	0	1.3	0.9	0	0.2	0.2	0.5	1.2	1.7
BSFC [g/kWh]	0.1	7.1	4.1	0.4	1.3	0.5	5.9	4.7	6.8

BSNOx [g/kWh]	0.01	0.06	0.12	0.02	0.04	0.21	0.06	0.10	0.27
BSSoot [g/kWh]	0.003	0.006	0.005	0.003	0.013	0.012	0.008	0.012	0.005
CA50 [CAD]	0.60	0.56	0.73	0.60	0.54	0.68	0.60	0.55	0.65

2 Combustion characteristics for low load operating conditions under the baseline calibration

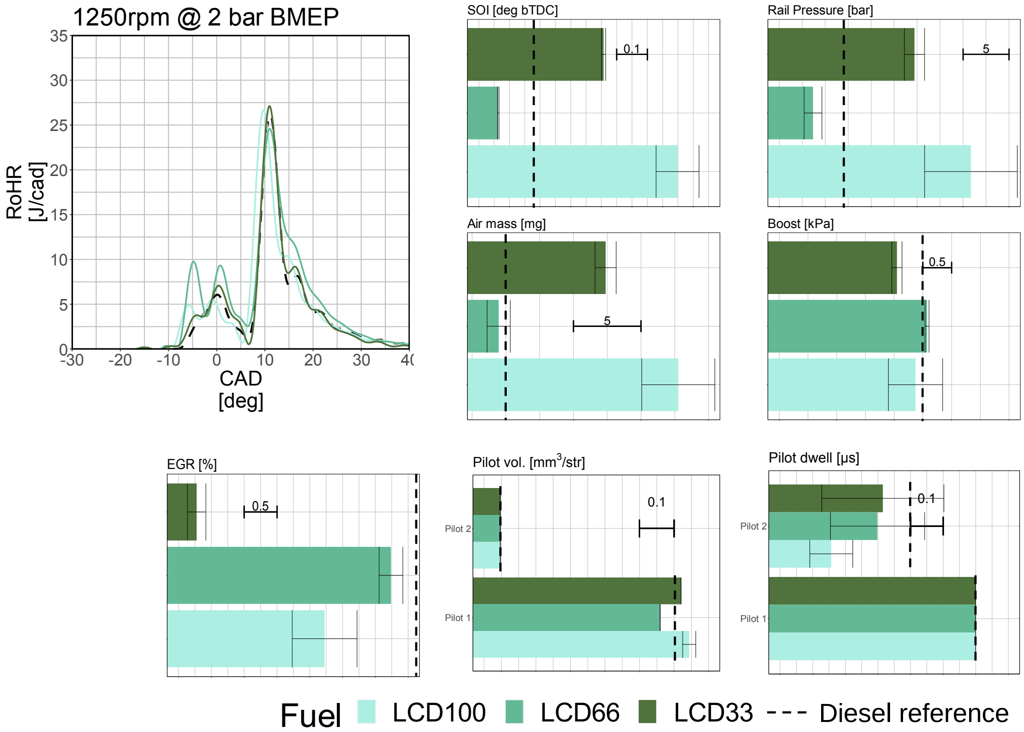

Figure 18 Effect of different LCF combustion on heat release rate with the baseline calibration for the operating condition 1250 rpm @ 2 bar

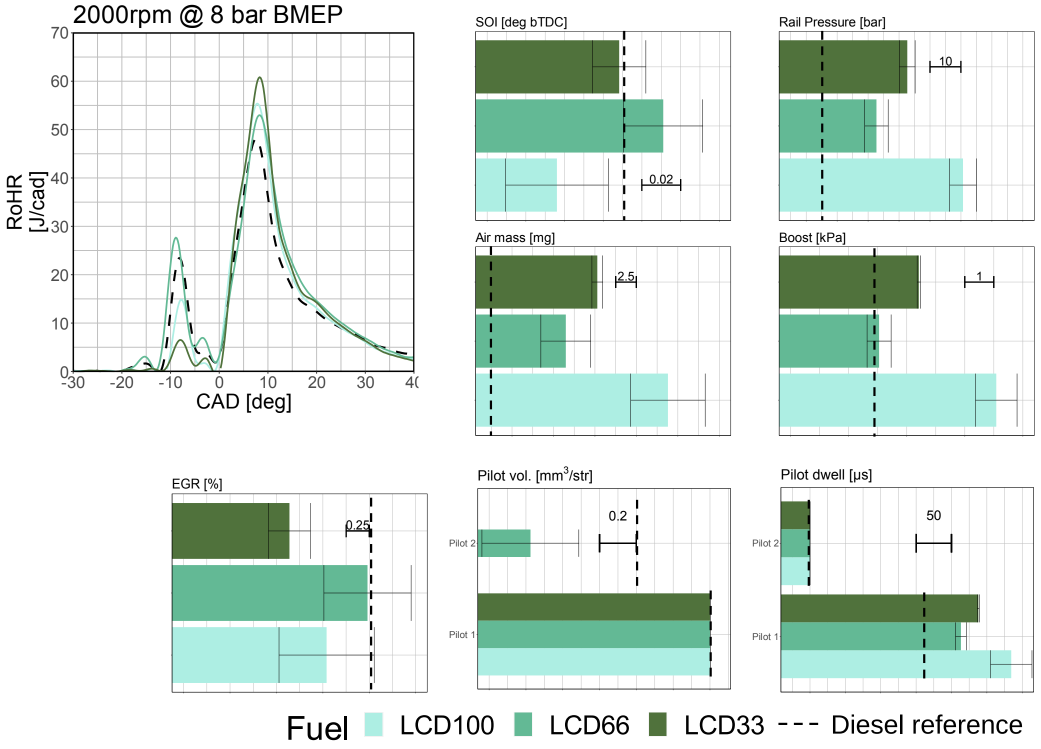

Figure 19 Effect of different LCF combustion on heat release rate with the baseline calibration for the operating condition 1250 rpm @ 2 bar